

Journal of Materials Chemistry C

Accepted Manuscript



This is an *Accepted Manuscript*, which has been through the Royal Society of Chemistry peer review process and has been accepted for publication.

Accepted Manuscripts are published online shortly after acceptance, before technical editing, formatting and proof reading. Using this free service, authors can make their results available to the community, in citable form, before we publish the edited article. We will replace this *Accepted Manuscript* with the edited and formatted *Advance Article* as soon as it is available.

You can find more information about *Accepted Manuscripts* in the [Information for Authors](#).

Please note that technical editing may introduce minor changes to the text and/or graphics, which may alter content. The journal's standard [Terms & Conditions](#) and the [Ethical guidelines](#) still apply. In no event shall the Royal Society of Chemistry be held responsible for any errors or omissions in this *Accepted Manuscript* or any consequences arising from the use of any information it contains.

Hybrid resist hemispherical-pit arrays layer for light trapping in thin film silicon solar cells via UV nanoimprint lithography

Cite this: DOI: 10.1039/x0xx00000x

Peihua Wangyang,^a Yanchang Gan,^b Qingkang Wang*^a and Xuesong Jiang^b

Received 00th January 2012,
Accepted 00th January 2012

DOI: 10.1039/x0xx00000x

www.rsc.org/

In this paper, we reported the micromorph tandem solar cells coated with the hemispherical-pit (HP) arrays layer, which traps the light and consequently enhances the efficiency. The quartz mold for ultraviolet nanoimprint lithography (UV-NIL) was fabricated by combining the UV photolithography and wet-etching technology, and the HP arrays was then transferred on the tandem solar cells through UV-NIL. The HP arrays layer could simultaneously reduce the average reflectance of the tandem solar cell from 7.7% to 1.8%, and effectively enhance light trapping by scattering more incident light into the tandem solar cells. A relative improvement of efficiency of the tandem solar cell coated with the HP arrays layer is up to 4.1% as compared to the reference device. The current-voltage characteristics of the tandem solar cells as a function of incident angle were also investigated. The power conversion efficiency of the tandem solar cell coated with the HP arrays layer is always higher than that of the reference with the same incident angle. The results further show that the HP arrays layer can effectively decrease reflectance and scatter more incident light into the solar cells at larger angles not only for normal incidence but also for the obliquely incident light. The external quantum efficiency (EQE) of the tandem solar cells coated with the HP arrays layer was also investigated as well as the reference tandem solar cells. The possible physical mechanism behind the observation is also discussed in this work.

1 Introduction

To improve the power conversion efficiency (PCE) of the thin film silicon solar cells, a number of light trapping techniques have been investigated in order to manipulate light inside the absorber layers and increase the effective path length in the solar cells.^{1,2} Light trapping is frequently accomplished through the use of randomly roughened or periodically textured surfaces, such as transparent conductive oxides (TCO),³⁻⁸ diffractive grating structures,⁹⁻¹¹ photonic crystal structures¹²⁻¹⁶ and plasma structures,¹⁷⁻²³ either on the front or rear of the solar cells. Generally, about 10% of incident light is reflected from the surface of the thin film silicon solar cells back to the air. However, the thin film silicon solar cells coated with an antireflection (AR) layer can significantly reduce the total light reflection and increase light absorption.²⁴⁻³¹ Especially, Escarré and coworkers³¹ demonstrated that the imprinting of random square based pyramidal textures can simultaneously enhance light in-coupling and light-trapping in amorphous silicon/microcrystalline silicon tandem solar cells, and the PCE is enhanced by 5% compared to the reference solar cells.

In addition, Yu and coworkers^{14,15} demonstrated that the hemispherical-pit arrays have a higher enhancement factor compared to hemispherical-concave arrays, and both textured arrays are performed under the condition that the hemispherical

diameter is equal to the array periodicity, so we design and fabricate a hybrid resist hemispherical-pit (HP) arrays layer (for convenience, the hybrid resist hemispherical-pit (HP) arrays layer is briefly named the HP arrays layer.) to enhance the PCE of the micromorph tandem solar cells via ultraviolet nanoimprint lithography (UV NIL) in this paper. The advantages of this technique are as following: the micromorph tandem solar cell is becoming one of the most promising candidates in terms of PCE through the combination of an amorphous silicon (a-Si:H) top cell having high band gap (1.7 eV) and a microcrystalline silicon (c-Si:H) bottom cell with low band gap (1.1 eV), which is extremely close to the theoretical values for the ideal tandem solar cells with maximum conversion efficiency.^{32,33} The UV-NIL is a low cost and relatively high throughput method for patterning nanostructures, which allows for mass production with step and repeat techniques.^{34,35} Moreover, compared with a traditional single AR layer, the HP arrays layer having a gradient refractive index can reduce the reflectance and scatter more incident light into the cells and prolong the optical path length.^{24,26} The other important benefit of this design is that it provide some room to reduce the thickness of the top a-Si:H absorber, thereby reducing the Staebler-Wronski degradation effect^{36,37} and thus leading to higher stability of the efficiency of the entire micromorph tandem solar cells.

Herein, we will introduce a novel technological process for making a quartz mold used in UV NIL. Then we focus on the fabrication of the HP arrays layer for the micromorph tandem solar cells via UV NIL. By varying the incident light angle under standard test conditions (25°C, AM1.5G and 100 mW/cm²), optical properties and tandem solar cells performance are discussed. The possible physical mechanism behind the observation is also explored in this work.

2 Experimental

2.1 Thin film solar cell fabrication

The fabricated process of the micromorph tandem thin film silicon solar cells was as follow. Firstly, a front contact F-doped SnO₂ layer with a thickness of 400 nm was deposited on bare glass substrate by atmosphere pressure chemical vapor deposition (APCVD).³⁸ Secondly, a front 200 nm thick a-Si (p-i-n) cell and a bottom 1800 nm thick μ -Si (p-i-n) cell with a 20 nm P-doped nc-SiO_x:H intermediate reflector in between were grown by the conventional plasma enhanced chemical vapor deposition (PECVD) technique. Finally, a thin ZnO:Al/Ag film serving as a back reflector was sputtered.

2.2 Materials and methods

The hybrid resist comprising fluorinated mercapfrontropy polyhedral oligomeric silsesquioxane (POSS-F-SH) and a diluted crosslinker (2,2,3,3,4,4,5,5-octafluoro-1,6-hexyl diacrylate, DCFA4) (POSS-F-SH/DCFA₄, and mole ratio, 1:16) was used as the material of the soft mold and the HP arrays layer because of its favorable properties, which include elastomeric character, low price, high optically transparency

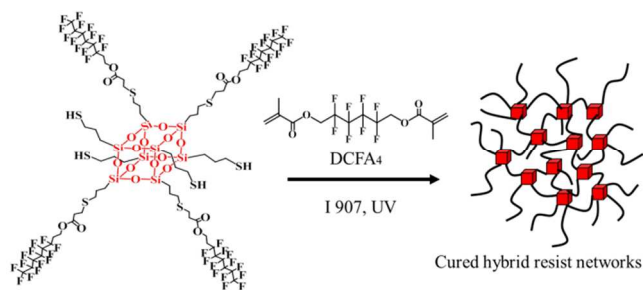


Fig. 1 Structures of hybrid resist based on thiol-ene photopolymerization.

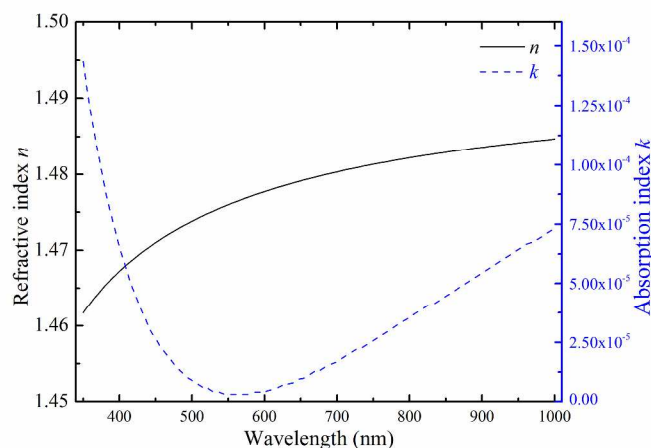


Fig. 2 The refractive index, n , and absorption index, k of hybrid resist.

(about 98% transmission above 350 nm), excellent mechanical property (Young's modulus: 627 MPa), low surface energy (18.8 mJ/m²), high decomposition temperature (335°C), and easy de-molding. Fig. 1 shows the structures of thiol-ene photocurable hybrid resist (POSS-F-SH/DCFA₄). The refractive index (n) and absorption index (k) of hybrid resist were measured using an NKD-8000 (Aquila, UK), as shown in Fig. 2. The detail synthetic process and characteristics of hybrid resist can be found in our previous report.³⁹

Many research works show that the considerably better performance is achieved by optimized textured surfaces.^{10, 14, 15} Especially, there have been studies demonstrating that optimized nanostructures can achieve the enhancement factor beyond the Yablonovitch limit.^{10, 40, 41} Here, we use a commercial mask with a pitch of 10 μ m and diameter hole of 5 μ m for UV photolithography. It should be noted that the texture of mask is not optimal, but commercially available and state of our art laboratory standard.

Fig. 3 shows the fabrication process flow of this work. The surface of a quartz substrate was firstly cleaned up with ACE, IPA, and D.I. water by ultrasonic agitation. A 100 nm Cr was deposited on the surface of the quartz substrate as the mask for wet etching. The quartz substrate with Cr layer was then spin-coated with AZ4620 photoresist and exposed to the UV exposure (Karl Suss MA6, Germany), as shown in Fig. 3(a). After developed with AZ 400MIF developer solution (Fig. 3(b)), the AZ4620 photoresist patterns were firstly chemically etched in a solution mixture of Ce(NH₄)₂(NO₃)₆, HClO₄, and D.I. water (9:6:85, by weight) for 60s to transfer the pattern onto the Cr layer shown in Fig. 3(c). After removing the photoresist, the entire quartz substrate with patterned Cr layer was dipped into the buffered hydrofluoric (BHF) acid solution mixture with 40%NH₄F and 49% HF for 3-5 min at 25°C. Thereafter removing Cr layer, the quartz mold with HP arrays can be obtained, as shown in Fig. 3 (e) and (f). Due to isotropic etching time of BHF solution, the wet etching process resulted in different textured HP arrays as shown in Fig. 4(a) and (b).

The surface of the quartz substrate (soft mold substrate) and the quartz mold with HP arrays were hydrophilic by immersing it in a piranha solution (30%H₂O₂: 98%H₂SO₄ = 1:3) at 150°C for 3h. After washing and drying, the quartz substrate of soft mold was soaked in 0.2 wt% MAPTES (3-(methacryloyloxy)propyltrimethoxysilane) in toluene solutions for 4 h, while the quartz mold was soaked in 0.2 wt% TCMTS ((5,5,6,6,7,7,8,8,9,9,10,10,10-tridecafluoro-4-methyldecyl) trimethoxy silane) in toluene solutions for 4h. Then both were cleaned thoroughly with fresh ethanol in an ultrasonic bath and dried in nitrogen gas, respectively. Thereafter the hybrid resist was spin-coated on the surface of quartz substrate of the soft mold at 1000 rpm for 15 s, and the thickness of the hybrid resist was about 5 μ m. Then the quartz substrate with the hybrid resist layer was covered by the quartz mold with HP arrays modified by the TCMTS molecules, as shown in Fig. 3(g). Finally, the sample was exposed to UV light for 10 min after a pressure of 0.02 MPa kept for 10 min by our home-made UV pneumatic imprinting machine (Fig. 3(h)). After de-molding, the quartz substrate (soft mold) with the patterned hybrid resist layer was baked at 100°C for 1 h to enhance its mechanical properties and solvent resistance.

Fig. 3 (j)-(l) shows the schematics fabrication of the HP arrays layer for the micromorph tandem solar cells. Before the hybrid resist was spin-coated on the surface of glass substrate

of the micromorph tandem solar cells, the surface of glass substrate of the micromorph tandem solar cells was suspended and immersed in 0.2 wt% MAPTES in toluene solutions for 4 h, then the surface of glass substrate was washed gently with ethanol to remove physisorbed MAPTES molecules, and dried with the nitrogen gas. Next, a 5 μm thick hybrid resist was spin-coated over the micromorph tandem solar cells at 1000 rpm for

15 s, and then the tandem solar cells with the hybrid resist layer and the soft mold were then combined and exposed to UV light for 6 min after a pressure of 0.02 MPa for 10 min, as illustrated in Fig. 3(k). After curing under UV light and de-molding, the surface of glass substrate of the micromorph tandem solar cells coated with the HP arrays layer can be obtained, as shown in Fig. 3(l).

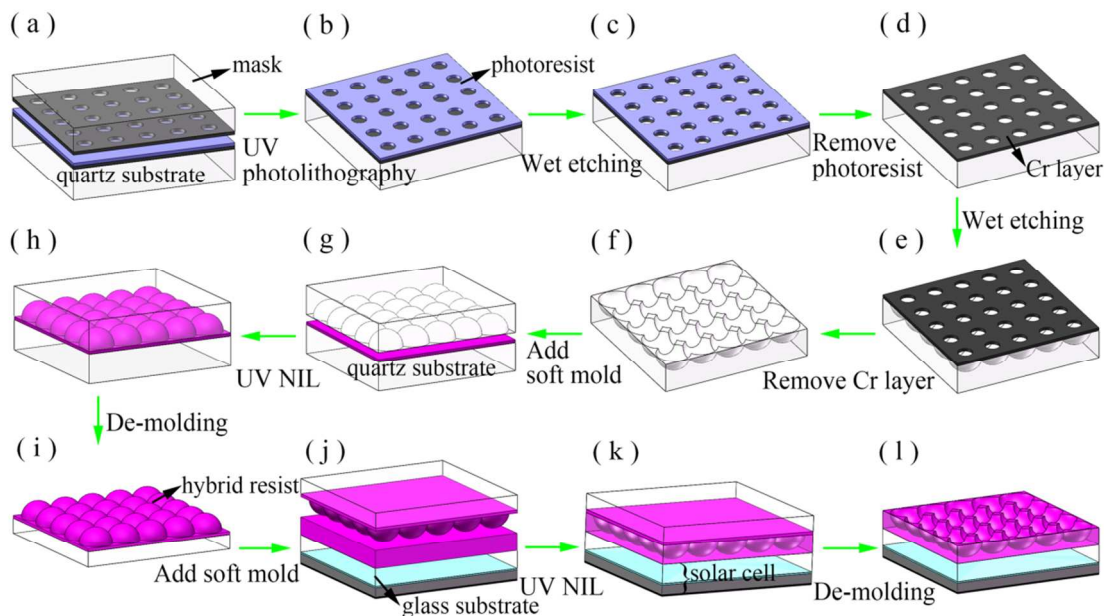


Fig. 3 Schematics and flow chart of the HP arrays layer making processes. (a)-(f) the fabrication process of quartz mold using the UV photolithography and wet etching, (g)-(i) the fabrication process of soft mold by UV NIL and (j)-(l) illustration of surface textured micromorph tandem solar cells coated with the HP arrays layer.

2.3 Characterization techniques

The microstructure of the samples was studied with a field emission scanning electron microscope (SEM) (ULTRA 55, Carl Zeiss AG, Germany). In all cases, a sputtered gold-palladium coating of 50 – 80 \AA was used to improve sample conductivity, as shown in Fig. 4(a)-(b). All surface images of the sample were obtained using sample mounts with a 30 degree inclination from the horizontal.

The reflectance from the surface of glass substrate of the micromorph tandem solar cells were measured using a UV/VIS/NIR spectrophotometer (Lambda-1050, Perkin Elmer) at room temperature, with an integrating sphere attachment over the spectral range of 300–1200 nm. All samples were measured at square spots of 4 mm \times 4 mm to obtain an average reflectance. Photocurrent of the tandem solar cells tested was analyzed using a solar simulator under Air Mass 1.5 Global (AM 1.5G) illumination condition (100 mW/cm 2 , 25 $^\circ$ C). The external quantum efficiency (EQE) of the tandem solar cells was also measured using a QEX10 quantum efficiency measurement system (PV Measurements).

3 Results and discussion

3.1 Surface characterization of the HP arrays layer

Fig. 4(a) and (b) show the SEM image of the quartz mold with different tapered HP arrays. A SEM image of the replica soft mold imprinted by the quartz mold (b) is also given in Fig. 4(c). Finally, the HP arrays layer having gradient refractive index is uniformly imprinted onto a surface of glass substrate of the micromorph tandem solar cells, which have a period of 10 μm and a depth of about 5 μm (not shown), as shown in Fig. 4(d). One can see that the pattern transferred on the light entrance surface of glass substrate of the micromorph tandem solar cells after two processes is still consistent well with the quartz mold.

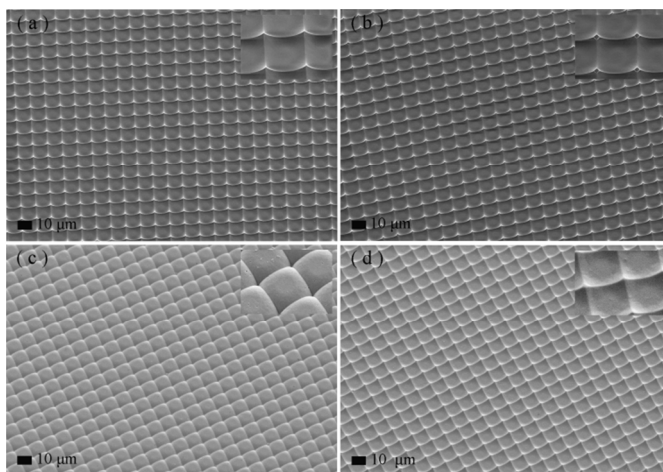


Fig. 4 SEM images of the quartz mold with different tapered HP arrays of (a) and (b). (c) SEM image of the replica soft mold imprinted by the quartz mold (b), and (d) SEM image of the tandem solar cell coated with the HP arrays layer imprinted by the replica soft mold (c).

3.2 Optical properties of the HP arrays layer

The reflectance of the tandem solar cells with three different typed texturing on the glass substrate was also measured using a UV/VIS/NIR spectrophotometer at room temperature. Fig. 5(a) shows the measured reflectance of the tandem solar cells coated with the hybrid resist layer (the thickness was about 5 μm) without and with the HP arrays at 8° tilted angle with respect to the normal incident light beam, and the tandem solar

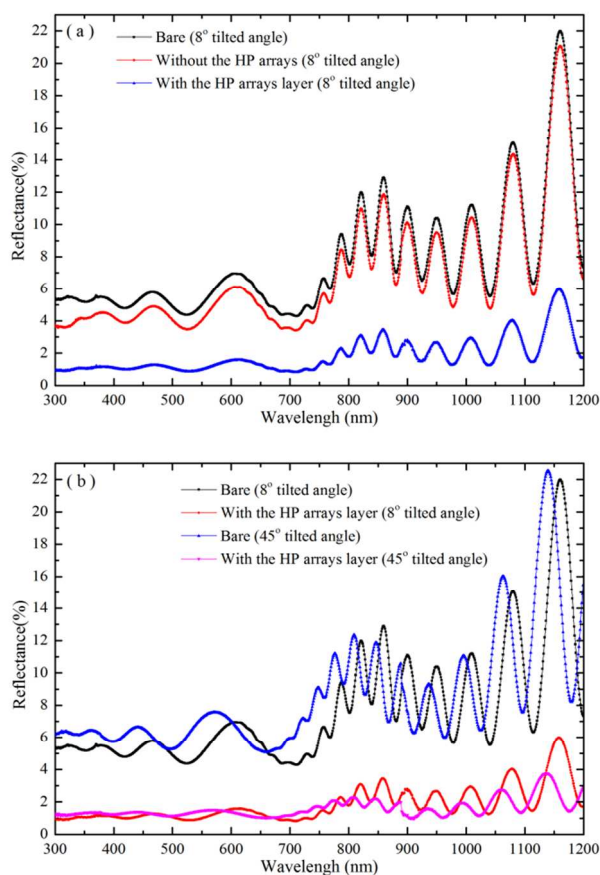


Fig. 5 (a) Measured reflectance of tandem solar cell devices with three different typed surface glass substrate (bare surface, coated the hybrid resist layer without the HP arrays, and coated with the HP arrays layer) under incident degree of 8° (Lambda-1050 limited). (b) Measured reflectance of tandem solar cell coated with the HP arrays layer under incident degree of 8° and 45°, and the bare tandem solar cell also displayed in parallel for comparison.

cells with the bare glass substrate served as reference. It is worth mentioning that a thin ZnO:Al/Ag film is placed on the backside of the solar cells as a perfect reflector mirror. So the transmission is approximated to be zero, and reducing the reflection means enhancing the absorption. Note that the strong oscillations of the spectra due to the interference between different interface of the bare solar cell, especially in the range

from 750 nm to 1200 nm. Meanwhile, it can be seen that the existence of HP arrays results in weaker interference and weaker intensity of the reflected wave. The average reflectance (averaged from 300 to 1200 nm) of the bare surface of the glass substrate was 7.7%. However, the tandem solar cells coated with the hybrid resist layer without and with the HP arrays structures had an even lower average reflectance of 6.8% and 1.8%, respectively. The reflectance of the tandem solar cells coated with the hybrid resist layer without the HP arrays also a little bit lower than that of the bare reference due to the lower refractive index of the hybrid resist layer material compared with that of the glass substrate. From Fig. 5(b), note that the reflectance of the tandem solar cells with the bare glass substrate increase with increasing the incident angle, however, for the tandem solar cells coated with the HP arrays layer, with increasing the incident angle, the reflectance increase below the wavelength of 800 nm and decrease from wavelength of 800 to 1200 nm. Compared with the traditional AR layer, the continuous change of the effective refractive index between air and the underlying glass is essential for suppressing light reflection.

3.3 Analysis of optics in the HP arrays layer

For the HP arrays layer, both scattering and diffraction will happen and make contribution to the absorption. And the diffraction arises from the collective interaction with many scattering objects. However, scattering effects dominate the absorption enhancement behavior due to the structure of the focused HP arrays larger than the incident light. Herein, the HP arrays layer was analyzed by geometrical optics in this work.³¹ For easy analysis of ray dynamic, the refractive index of the hybrid resist and the glass substrate of the tandem solar cells are fixed to be 1.478 at wavelength of 600 nm due to a quite close of the refractive index between the hybrid resist and the glass substrate of the tandem solar cells. In addition, the transparent conductive oxide layer with random texture was under the glass substrate (not shown). Fig. 6(a) shows how the incident light interacts with the hybrid resist without (left) and with (right) the HP arrays layer. By applying Snell's law, the incident light which is perpendicularly projected onto the hybrid resist without the HP arrays layer have been divided into two parts. Part of the light will enter into the solar cells, and the other part will be reflected back to the air. While the normal incident light projected onto the HP arrays layer also have been divided into two parts. One part of the light will be refracted into the HP arrays layer with different direction of propagation, and the other part may travel towards the HP arrays again or back towards the air. For example, when $\alpha_1 = 60^\circ$, one can get

$\alpha_2 = 35.87^\circ$ and most of the incident light is refracted into the tandem solar cells. Such result shows that the HP arrays layer can scatter more incident light into the tandem solar cells and prolong the optical path length even though the obliquely incident light.

The ray diagrams of Fig. 6(b) shows how the outgoing light interacts with the HP arrays layer. According to the Snell refraction law, the total internal reflection will happen if the incident angle is larger than the critical angle. The critical angle should satisfy Eq. (1) and the total reflection condition of the HP arrays layer should satisfy the angle – side Eq. (2) of the triangle, as shown in the following.

$$n_i \sin \theta_c = 1 \quad (1)$$

$$\sin\delta = \frac{R}{R+L+H} \cdot \sin\beta \approx \frac{R}{R+H} \cdot \sin(180^\circ - \theta) \quad (2)$$

Where $n_i = 1.478$ is the refractive index of the hybrid resist at wavelength of 600 nm, one can get the critical angle $\theta_c = 42.58^\circ$. $R = 5 \mu\text{m}$ is the radius of the HP arrays, L is the height of the hybrid resist between the HP arrays and the glass substrate (L is small and can be negligible here), and $H = 1000 \mu\text{m}$ is the height of the glass substrate. For the hybrid resist without the HP arrays layer, when $a_4 = \theta_c = 42.58^\circ$, one can get $a_3 = 90^\circ - a_4 = 90^\circ - \theta_c = 47.42^\circ$, that means part of the

scattered light with the angle bigger than $a_3 = 47.42^\circ$ will escape from the solar cells. However, according to the Eq. (2), However, according to the Eq. (2), the scattered light with the angle range from 0° to 89.81° (when $\theta = \theta_c$, then $0^\circ < a_5 < 90^\circ - \delta = 90^\circ - 0.19^\circ = 89.81^\circ$) will experience internal total reflection for the tandem solar cells coated with the HP arrays layer. Such results demonstrate that the HP arrays layer can make more outgoing light reflect back into the tandem solar cells compared with that of the reference tandem solar cells coated with the hybrid resist layer without the HP arrays.

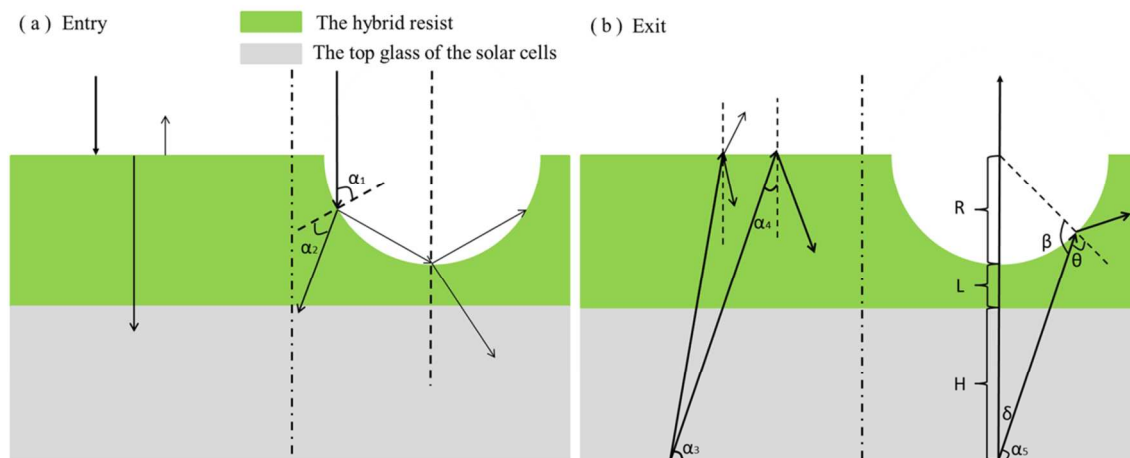


Fig. 6 Ray diagrams showing how light geometrically interacts with the HP arrays texture when (a) entering or (b) exiting the device.

3.4 Efficiency of tandem solar cells coated with the HP arrays layer

Firstly, five bare samples were tested using a solar simulator under AM 1.5G illumination condition before spin-coating the hybrid resist layer. For the sake of comparison, the samples 1-4 coated with the HP arrays layer and sample 5 coated with the hybrid resist layer without the HP arrays were also tested. The performance and I-V characteristics of all five samples are presented in Table 1. The short circuit current density (J_{sc}) of sample 1-4 has been enhanced after introducing the HP arrays layer. While the short circuit current density (J_{sc}) of sample 5 coated with the hybrid resist layer without the HP arrays also a little bit higher than that of the bare reference. A relative improvement of efficiency of the tandem solar cell (sample 1) coated with the HP arrays layer is up to 4.1% as compared to the reference device, which is agreed well with the theoretical calculation.³⁷ But it is lower than that the predicted enhancement by reducing reflectance. Such phenomena can be explained as follows: on the one hand, the AM 1.5G spectrum is nonlinear and nonuniform distribution, which could not guarantee the same increment to the tandem solar cells like the UV/VIS/NIR spectrum, on the other hand, the increments of short circuit current density of top cell and bottom cell of the tandem solar cells are different, and thus part photo-generated carriers of the cell with the greater short circuit current density will recombine

again. In addition, the absorption of the hybrid resist layer also leads to low power conversion efficiency (especially, below 350 nm).³⁹ However, no doubt that the coated HP arrays layer has a gradient refractive index, which can reduce the reflectance and scatter more incident light into the cell induced by ordered HP arrays and prolong the optical path length,^{24,26} therefore enhancing the light trapping and boosting light conversion efficiency for the micromorph tandem solar cells.

In order to evaluate the influence of the oblique light incidence condition, current-voltage characteristics of the tandem solar cell (Sample 1) as a function of incident angle was further investigated, and the corresponding bare sample was served as reference, as shown in Table 2. In addition, the I-V characteristics of sample 1 before and after adding the HP arrays layer under incident angle of 0° and 45° were also given in Fig. 7. From table 2 and Fig. 7, one can see that both short circuit current density (J_{sc}) and open circuit voltage (V_{oc}) are decrease with increasing the incident angle due to the weakness of solar energy density spectrum into the tandem solar cells. It is worth noting that PCE of sample 1 coated with the HP arrays layer is always higher than that of bare sample 1 with the same incident angle. As discussed above, such behaviour further indicates that the coated HP arrays layer can effectively scatter more incident light into the solar cells at larger angles not only for normal incidence but also for obliquely incident light, therefore improving the short circuit current density and thus leading to higher light conversion efficiency.

Table 1. Current-voltage characteristics of power conversion efficiency (PCE), short circuit current density (J_{sc}), open circuit voltage (V_{oc}), and fill factor (FF) at AM 1.5G of the tandem solar cells coated with the HP arrays layer. The corresponding bare samples and the sample5 coated with the hybrid resist layer without the HP arrays served as reference.

Sample		PCE(%)	J_{sc} (mA/cm ²)	V_{oc} (V)	FF(%)
Sample1	Bare	8.321	10.86	1.276	60.06
	With the HP arrays layer	8.662	11.30	1.275	60.12
Sample2	Bare	8.148	10.43	1.275	61.27
	With the HP arrays layer	8.381	10.76	1.278	60.95
Sample3	Bare	8.442	10.94	1.275	60.52
	With the HP arrays layer	8.768	11.23	1.271	61.43
Sample4	Bare	8.396	10.84	1.276	60.70
	With the HP arrays layer	8.738	11.13	1.279	61.38
Sample5	Bare	8.201	10.00	1.280	64.07
	Without the HP arrays	8.264	10.18	1.278	63.52

Table 2. Current-voltage characteristics of PCE, J_{sc} , V_{oc} , and FF at AM 1.5G under different incident angle of tandem solar cell (Sample1) coated with the HP arrays layer. The corresponding bare samples are served as reference.

Sample1		0°	15°	30°	45°	60°
PCE(%)	Bare	8.321	8.172	7.593	6.487	4.632
	With the HP arrays layer	8.662	8.573	7.980	6.821	5.002
J_{sc} (mA/cm ²)	Bare	10.86	10.62	9.795	8.273	5.844
	With the HP arrays layer	11.30	11.13	10.27	8.698	6.378
V_{oc} (V)	Bare	1.276	1.273	1.269	1.264	1.248
	With the HP arrays layer	1.275	1.273	1.270	1.268	1.251
FF(%)	Bare	60.05	60.45	61.09	62.03	63.51
	With the HP arrays layer	60.12	60.51	61.18	61.85	62.69

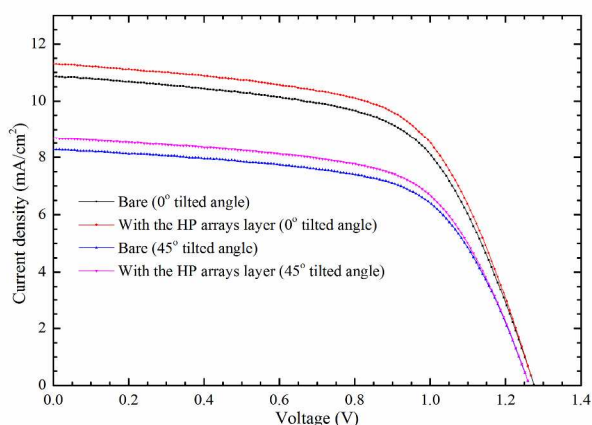


Fig. 7 I-V characteristics of sample1 before and after coating with the HP arrays layer under incident angle of 0° and 45°.

In order to further understand the enhancement absorption spectral range of the tandem solar cells after adding the hybrid resist layer with or without HP arrays. The EQE of the tandem solar cells with three different typed texturing on the surface of glass substrate was measured using a QEX10 quantum efficiency measurement system, as shown in Fig. 8. One can see firstly that the EQE of the bare tandem solar cells higher than that of the tandem solar cells coated with the hybrid resist layer with and without the HP arrays due to the low optically transparency (about 85%) below 350 nm,³⁹ while the EQE of the HP arrays layer higher than that of the hybrid resist layer without the HP arrays due to the lower effective thickness with the HP arrays. Note that the bare tandem solar cells and the tandem solar cells coated with the hybrid resist layer without the HP arrays exhibit almost equivalent EQE, top and bottom cell currents. Such phenomena can be explained that the hybrid resist material has a little bit lower the refractive index compared with that of top glass of the tandem solar cells, and

also served as a traditional AR layer. The tandem solar cells coated with the HP arrays layer, the currents increase from 10.98 to 11.43 mA/cm² for the top cell, and from 11.21 to 12.06 mA/cm² for the bottom cell, respectively. The relative increase of both top and bottom cells are 4.1% and 7.6%, respectively. The short circuit current density of the tandem solar cells depends on the lower current (the J_{sc} of top cell), and the increase of the J_{sc} of top cell by EQE agrees well with the enhancement of Fig. 7. Such results also indicate that the bottom cell benefits more from the HP arrays layer.

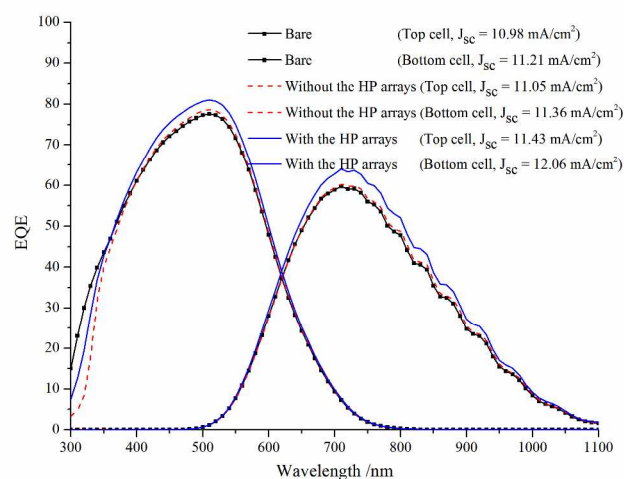


Fig. 8 External quantum efficiency curves of the tandem solar cells with three different typed surface of glass substrate (bare surface, coated with the hybrid resist layer without the HP arrays, and coated with the HP arrays layer).

For the micromorph tandem solar cells here, the HP arrays layer having a gradient refractive index not only provides excellent antireflection properties but also can effectively

scatter more incident light into the cell induced by ordered HP arrays and prolong the optical path length,^{24,26} therefore enhancing the light trapping and improving the short circuit current density. Although the bottom cell benefits more from the HP arrays layer, it could still supply some room to tailor the thickness of the front a-Si:H absorber, thereby reducing the Staebler-Wronski degradation effect^{36,37} and thus leading to higher stability of the efficiency of the entire micromorph tandem solar cells. In addition, although the surface morphology from V-shaped to U-shaped can improve the electrical device performances of deposited cells, it cannot guarantee that there is no cracks formed in the U-shaped valleys between the nanostructure arrays as the silicon layers growing on neighboring nanostructures collide.^{22, 42, 43} The cracks might cause degradation in V_{oc} and FF in the deposited cells. However, the HP arrays layer offer a means of improving the efficiency not by changing the microelectronics fabrication methods or altering the device chemistry, but by simply adding a coated hybrid resist layer with the HP arrays onto the glass substrate of the tandem solar cells. So the major advantage is that it avoided the formation of cracks during the growth of the layers, then the V_{oc} and FF are not affected by the backside structure, compared to other light trapping configurations such as textured silicon interface,^{22, 42, 43} and thus yielding better cell performance. This technique could also be implemented in the single silicon thin film solar cells for efficiency enhancement. We believe that, with further optimized parameters of the HP arrays, the performance of our HP arrays layer can more effectively enhance the PCE of the solar cells.

4 Conclusions

In this study, we have demonstrated a novel method for making a quartz mold for UV-NIL. The HP arrays layer was successfully applied on the surface of the glass substrate of the micromorph tandem solar cells via UV NIL. The HP arrays layer has effectively reduced the reflection and led to scattering more incident light into the micromorph tandem solar cells and prolong the optical path length, therefore increasing short circuit current density and enhancing PCE of tandem solar cells. Compared with that of 7.7% of the reference tandem solar cell, the average reflectance of the tandem solar cell coated with the hybrid resist layer without and with the HP arrays structures have dropped to 6.8% and 1.8%, respectively. A relative improvement of efficiency of the tandem solar cell coated with the HP arrays layer is up to 4.1% as compared to the reference device. Furthermore, the HP arrays layer could provide some room to reduce the Staebler-Wronski degradation effect and thus leading to higher stability of the efficiency of the entire micromorph tandem cells due to the fine trapping light performance. In addition, the HP arrays layer exhibited a hydrophobic nature due to the low surface energy of the hybrid resist with HP arrays. Another important benefit using the HP arrays layer on the surface of glass substrate of the solar cell is that it is useful to avoid the formation of cracks during the silicon growth. The results demonstrate that the HP arrays layer has great potential in solar cells applications.

Acknowledgements

This research is supported by National High-Tech Research and Development Program of China (State 863 Projects, Grant No. 2011AA050518).

Notes and references

^a Key Laboratory for Thin Film and Microfabrication Technology of Ministry of Education, Research Institute of Micro/Nano Science and Technology, Shanghai Jiao Tong University, Shanghai 200240, P.R.China. E-mail: wangqingkang@sjtu.edu.cn

^b School of Chemistry and Chemical Engineering, Shanghai Jiao Tong University, Shanghai 200240, P.R.China.

- J. Li, H. Yu and Y. Li, *Nanoscale*, 2011, **3**, 4888-4900.
- H.-P. Wang, D.-H. Lien, M.-L. Tsai, C.-A. Lin, H.-C. Chang, K.-Y. Lai and J.-H. He, *J. Mater. Chem. C*, 2014.
- J. Muller, B. Rech, J. Springer and M. Vanecek, *Sol. Energy*, 2004, **77**, 917-930.
- C. Battaglia, J. Escarre, K. Soderstrom, L. Erni, L. Ding, G. Bugnon, A. Billet, M. Boccard, L. Barraud, S. De Wolf, F. J. Haug, M. Despeisse and C. Ballif, *Nano Lett.*, 2011, **11**, 661-665.
- A. Bessonov, Y. Cho, S. J. Jung, E. A. Park, E. S. Hwang, J. W. Lee, M. Shin and S. Lee, *Sol. Energy Mater. Sol. Cells*, 2011, **95**, 2886-2892.
- S.-Y. Han, B. K. Paul and C.-h. Chang, *J. Mater. Chem.*, 2012, **22**, 22906-22912.
- T. Shinagawa, K. Shibata, O. Shimomura, M. Chigane, R. Nomura and M. Izaki, *J. Mater. Chem. C*, 2014.
- Y.-C. Chen, P.-Y. Su, S.-C. Tseng, Y.-C. Lee and H.-L. Chen, *J. Mater. Chem. A*, 2014, **2**, 4633-4641.
- L. Zeng, Y. Yi, C. Hong, J. Liu, N. Feng, X. Duan, L. Kimerling and B. Alamariu, *Appl. Phys. Lett.*, 2006, **89**, 111111-111113.
- X. Sheng, S. G. Johnson, J. Michel and L. C. Kimerling, *Opt. Express*, 2011, **19**, 841-850.
- M. Peters, M. Rudiger, H. Hauser, M. Hermle and B. Blasi, *Prog. Photovoltaics*, 2012, **20**, 862-873.
- R. Biswas, J. Bhattacharya, B. Lewis, N. Chakravarty and V. Dalal, *Sol. Energy Mater. Sol. Cells*, 2010, **94**, 2337-2342.
- X. Sheng, J. F. Liu, I. Kozinsky, A. M. Agarwal, J. Michel and L. C. Kimerling, *Adv. Mater.*, 2011, **23**, 843-+.
- J. S. Li, H. Y. Yu and Y. L. Li, in *Proceedings of the Silicon PV 2011 Conference*, 2011, 180-184.
- J. Li, H. Yu, Y. Li, F. Wang, M. Yang and S. M. Wong, *Appl. Phys. Lett.*, 2011, **98**, 021905.
- C. Battaglia, C. M. Hsu, K. Soderstrom, J. Escarre, F. J. Haug, M. Charriere, M. Boccard, M. Despeisse, D. T. L. Alexander, M. Cantoni, Y. Cui and C. Ballif, *Acs Nano*, 2012, **6**, 2790-2797.
- H. A. Atwater and A. Polman, *Nat. Mater.*, 2010, **9**, 865-865.
- V. E. Ferry, M. A. Verschuuren, H. B. T. Li, E. Verhagen, R. J. Walters, R. E. I. Schropp, H. A. Atwater and A. Polman, *Opt. Express*, 2010, **18**, A237-A245.
- V. E. Ferry, M. A. Verschuuren, M. C. van Lare, R. E. I. Schropp, H. A. Atwater and A. Polman, *Nano Lett.*, 2011, **11**, 4239-4245.
- H. R. Tan, R. Santbergen, A. H. M. Smets and M. Zeman, *Nano Lett.*, 2012, **12**, 4070-4076.
- M. G. Deceglie, V. E. Ferry, A. P. Alivisatos and H. A. Atwater, *Nano Lett.*, 2012, **12**, 2894-2900.
- C. M. Hsu, C. Battaglia, C. Pahud, Z. C. Ruan, F. J. Haug, S. H. Fan, C. Ballif and Y. Cui, *Adv. Energy Mater.*, 2012, **2**, 628-633.

- 23 M. J. Mendes, S. Morawiec, F. Simone, F. Priolo and I. Crupi, *Nanoscale*, 2014.
- 24 K. Hadobas, S. Kirsch, A. Carl, M. Acet and E. F. Wassermann, *Nanotechnology*, 2000, **11**, 161-164.
- 25 B. G. Prevo, E. W. Hon and O. D. Velev, *J. Mater. Chem.*, 2007, **17**, 791-799.
- 26 J. Y. Chen and K. W. Sun, *Sol. Energy Mater. Sol. Cells*, 2010, **94**, 629-633.
- 27 J. H. Shin, K. S. Han and H. Lee, *Prog. Photovoltaics*, 2011, **19**, 339-344.
- 28 K. S. Han, J. H. Shin, K. I. Kim and H. Lee, *Jpn. J. Appl. Phys.*, 2011, **50**, 020207-020210.
- 29 J. Y. Chen, W. L. Chang, C. K. Huang and K. W. Sun, *Opt. Express*, 2011, **19**, 14411-14419.
- 30 A. Basch, F. Beck, T. Soderstrom, S. Varlamov and K. R. Catchpole, *Prog. Photovoltaics*, 2012, **20**, 837-842.
- 31 J. Escarré, K. Söderström, M. Despeisse, S. Nicolay, C. Battaglia, G. Bugnon, L. Ding, F. Meillaud, F.-J. Haug and C. Ballif, *Sol. Energy Mater. Sol. Cells*, 2012, **98**, 185-190.
- 32 H. Keppner, J. Meier, P. Torres, D. Fischer and A. Shah, *Appl. Phys. A Mater. Sci. Process*, 1999, **69**, 169-177.
- 33 A. De Vos, *J. Phys. D: Appl. Phys.*, 2000, **13**, 839.
- 34 M. Colburn, S. Johnson, M. Stewart, S. Damle, T. Bailey, B. Choi, M. Wedlake, T. Michaelson, S. V. Sreenivasan, J. Ekerdt and C. G. Willson, in *Emerging Lithographic Technologies Iii, Pts 1 and 2*, 1999, 379-389.
- 35 M. Otto, M. Bender, F. Richter, B. Hadam, T. Kliem, R. Jede, B. Spangenberg and H. Kurz, *Microelectron. Eng.*, 2004, **73-4**, 152-156.
- 36 D. L. Staebler and C. Wronski, *Appl. Phys. Lett.*, 1977, **31**, 292-294.
- 37 J. Krc, F. Smole and M. Topic, *J. Non-Cryst. Solids*, 2006, **352**, 1892-1895.
- 38 U. Dagkaldiran, A. Gordijn, F. Finger, H. M. Yates, P. Evans, D. W. Sheel, Z. Remes and M. Vanecek, *Mater. Sci. Eng., B*, 2009, **159-60**, 6-9.
- 39 H. Lin, X. Wan, X. S. Jiang, Q. K. Wang and J. Yin, *J. Mater. Chem.*, 2012, **22**, 2616-2623.
- 40 Z. F. Yu, A. Raman and S. H. Fan, *Proc. Natl. Acad. Sci. U.S.A.*, 2010, **107**, 17491-17496.
- 41 D. M. Callahan, J. N. Munday and H. A. Atwater, *Nano Lett.*, 2012, **12**, 214-218.
- 42 M. Python, O. Madani, D. Domine, F. Meillaud, E. Vallat-Sauvain and C. Ballif, *Sol. Energy Mater. Sol. Cells*, 2009, **93**, 1714-1720.
- 43 M. Python, D. Dominé, T. Söderström, F. Meillaud and C. Ballif, *Prog. Photovoltaics*, 2010, **18**, 491-499.